Strake-Generated Vortex Interactions for a Fighter-Like Configuration

Steven G. Reznick*
U.S. Space Command Headquarters, Peterson Air Force Base, Colorado
and
Jolen Flores†
NASA Ames Research Center, Moffett Field, California

A combination of the Euler and thin-layer Navier-Stokes equations were solved for the flowfield around a wing-strake-fuselage configuration similar to the General Dynamics F-16A aircraft. Steady-state solutions were obtained at angles-of-attack ranging from 6 to 10 deg at $M_\infty = 0.3$, 0.6, and 0.9, and Reynolds numbers matching those of wind-tunnel and water-tunnel experiments. The flowfield was divided into multiple blocks using a zoning program and the transonic Navier-Stokes wing-fuselage (TNSWF) solution program, based on an implicit solution algorithm, which updates each subregion of the flowfield sequentially. The total grid contained approximately 300,000 grid points, and clustering was affected normal to all aircraft surfaces. The computed solutions agreed well quantitatively with wind-tunnel pressure distribution data, and they agreed well qualitatively with flow visualization from wind- and water-tunnel tests.

Introduction

FOR many years, a goal of computational aerodynamicists has been to compute accurately the fluid flow around highly maneuverable aircraft configurations at transonic speeds. The attainment of this goal requires solving the proper equation set within an adequately fine grid to capture correctly the significant physical flow phenomena. This paper describes the computation of subsonic and transonic flow around a wind-strake-fuselage body, derived from the General Dynamics F-16A aircraft. This approach utilizes a combination of the Euler and the thin layer form of the Navier-Stokes equations, for both laminar and turbulent cases. These solutions portray the strake-vortex interaction with the wing flow, and other appropriate flow features at moderate angles of attack.

Questions regarding the proper design and employment of strakes and canards were summarized by Peake and Tobak[1] and concern the concepts of properly understanding the structure and mechanisms of three-dimensional separations and the resulting vortical development. How these vortical mechanisms react with each other and with boundary layers, especially under the influence of shock waves, is critical to both their control and eventual breakdown in transonic flight.

There is a need for employing the Navier-Stokes equations, which are computationally expensive and complicated to apply, to complete aircraft configurations. It is required by the design effort to improve maneuvering performance using the nonlinear-type lift generated by a strake [also called leading-edge extension (LEX)] or canard. This inducement of an inboard vortex allows maintainable and controllable lift high above the angles of attack at which a wing, conventionally designed for attached flow, would have stalled. In the recent past, the application of linear and nonlinear panel-type methods has become adequate and cost-effective to solve the necessary flowfields for the design of commercial transports over their limited performance range.[2,3] Solutions for more exotic geometries have been computed using the nonlinear, full-potential equations.[4] However, the underlying assumptions of isentropic and irrotational flow make potential-flow approaches inadequate for capturing vortices and their interaction with the strong shock waves encountered in the problems of current interest. Although the Euler equations are adequate to capture nonisentropic phenomena such as strong shocks, their ability to capture vortex formation properly is questioned.[5,6] Furthermore, Westphal et al.[7] postulate that viscous interaction with the boundary-layer significantly affects the shape of weak streamwise vortices, as well as their burst point. The boundary-layer equations have proven adequate to capture viscous effects for moderately separated flows, but the inability of these schemes to transmit vorticity to the inviscid zones at the interface prevents strake-vortex capture. Thus, the solution of vortex/separation-region interactions complicated by strong shock effects requires some form of the Navier-Stokes equations.

Grid and Solution Equation Set

The equation sets employed in the Transonic Navier-Stokes (TNS) project are the Euler and Reynolds-averaged Navier-Stokes equations, utilizing the thin-layer assumption suggested by Baldwin and Lomax and first employed by Steger.[8,9] These equations are embodied in Pulliam's[10] ARC (Ames Research Center) three-dimensional solution kernel, which is based on the Beam-Warming[11] implicit numerical method for compressible solutions. This was modified by Pulliam and Chaussee[12] to a scalar diagonalized inversion matrix for improved solution efficiency. The Baldwin-Lomax turbulence model[8] is utilized to calculate turbulent eddy viscosity. Further information on the solution process can be gained by examining the Flores[13] paper concerning convergence acceleration for TNS wing-alone solutions, and Hung and MacCormack's[14] application of the thin-layer approximation in two directions, which was subsequently adopted for use in the transonic Navier-Stokes wing-fuselage (TNSWF) code.

The grid construction is a natural progression of a zonal approach developed by Holst et al.,[15] Flores et al.,[16] and Kaynak et al.[17] for the solution of flows about three-dimensional wings, in which a coarsely spaced flowfield is subdivided into two types of zones. Zones adjacent to the surface are treated as viscous, and clustering is provided normal to the surface. The remaining zones, away from the surface, retain coarse spacing and flow in these zones is treated as inviscid. This subdivision was accomplished with four zones for three-

Presented as Paper 87-0589 at the AIAA 25th Aerospace Sciences Meeting, Reno, NV, Jan. 12–15, 1987; received April 20, 1987; revision received May 2, 1988. This paper is declared a work of the U.S. Government and therefore is in the public domain.

*Major, United States Air Force. Member AIAA.
†Research Scientist. Member AIAA.

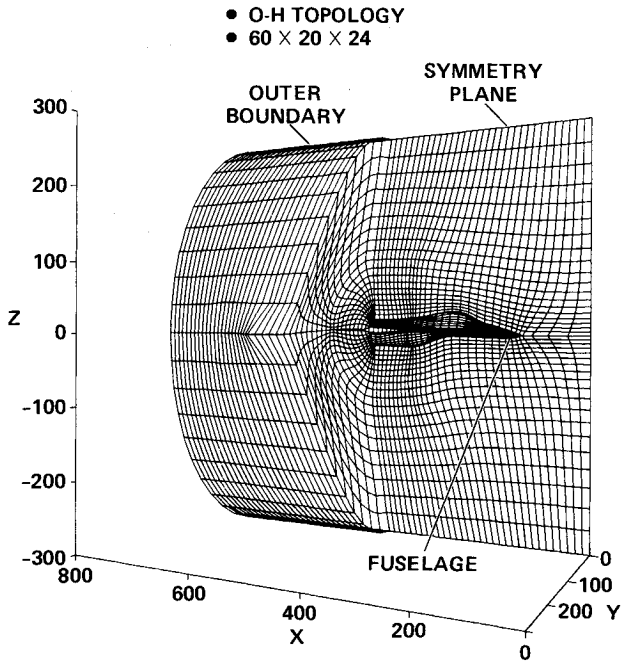

Fig. 1 Elliptically generated base flowfield grid.

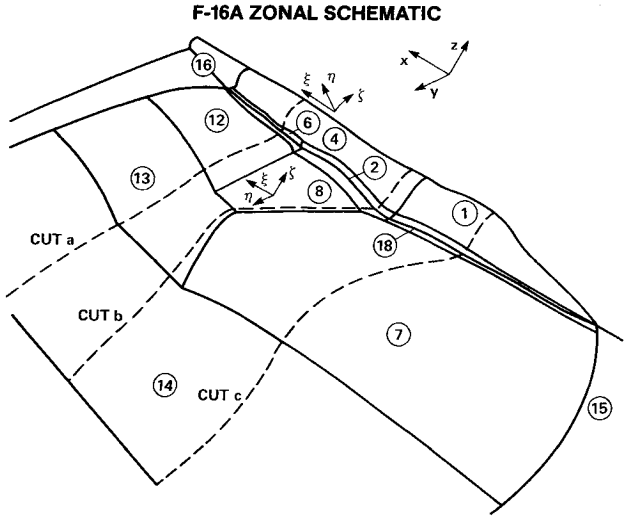

Fig. 2 Schematic of zonal boundaries on the aircraft surface and in the plane containing the wing chord lines.

dimensional wings. However, for the wing-strake-fuselage F-16-like geometry considered here, 18 zones were required (Figs. 1 and 2). Sixteen zones were designated initially, but two zones were added to refine the grid near the strake edge in order to capture the strake vortex suction peak properly. This geometry represents the correct surface for the General Dynamics F-16A fighter aircraft,[18] with the exceptions that the inlet is faired over and the tail surfaces are removed. The surface definition required 8400 points to represent the fuselage and 4600 points to model the wing. The coarse flowfield grid, depicted in Fig. 1, contained approximately 30,000 points.[19] After the ZONER program was used to subdivide the grid and cluster points normal to the aircraft surface (Fig. 2), the flowfield grid contained a total of 304,000 points. It is anticipated that grids containing 500,000 points will be required to represent geometries that include the flowthrough inlet and exhaust and the omitted tail surfaces. To obtain the solution, the applicable equation set is updated in each zone sequentially. Flowfield data for a given zone is brought into the central memory and advanced one time step. Boundary information along common grid boundaries is then passed to adjacent zones. These solutions were computed on the NASA Ames Cray XMP/48, and the flowfields were examined using graphics workstations and the NASA Ames Cray 2. The TNSWF code currently requires approximately 16 s to advance the solution one iteration, depending on number of zones employed, use of turbulence model, etc. Efficient programming was of secondary concern while obtaining these pioneering solutions. Thus, it is anticipated that significant reductions in computer time will be attained through code vectorization enhancements. In addition, the TNSWF code is being converted for operation on the Cray 2, which will allow finer grids because of its expanded main memory.

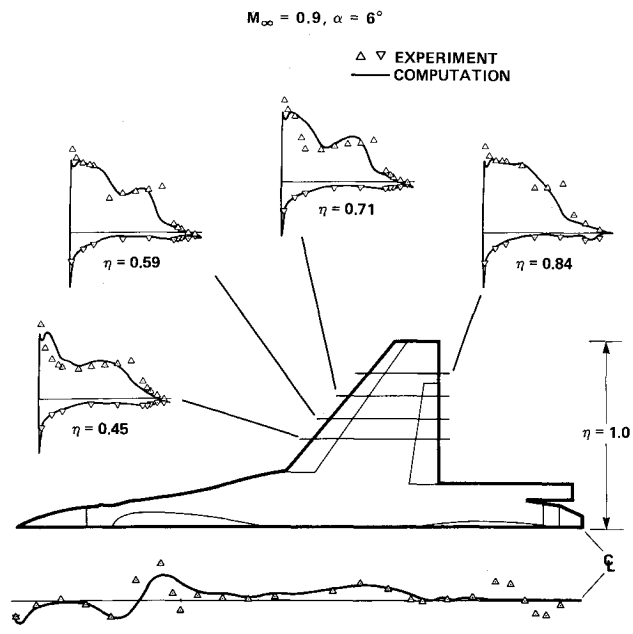

Fig. 3 Coefficient of pressure (C_p) comparisons for the $M_\infty = 0.9$, $\alpha = 6.15$ deg, $Re = 4.5 \times 10^6$ turbulent solution.

Results

The first solution presented is for turbulent flow at $M_\infty = 0.9$, $\alpha = 6$ deg, and Reynolds number (based on wing-root chord) $Re = 4.53 \times 10^6$. These conditions were chosen to match available wind-tunnel data.[20] The other solutions are for laminar flow, obtained using a slightly coarser grid, at $M_\infty = 0.3$ and 0.6, $\alpha = 10$ deg, and $Re = 1.5 \times 10^4$. The low Reynolds number was chosen to match that of an available water-tunnel test.[21] In addition, a quasilaminar case was run at $M_\infty = 0.6$, $\alpha = 10$ deg, and $Re = 8.0 \times 10^6$. This was done because a fine-grid turbulent solution has not yet been converged at $\alpha = 10$ deg, because of numerical instabilities caused by the sharp leading edge. A comparison to the low Re solution with other parameters held constant can also be made.

Turbulent Case, $M_\infty = 0.9$, $\alpha = 6$ deg

This solution took approximately 3200 iterations at a cost of 16 h of Cray XMP CPU time to achieve 3 to 5 orders of magnitude drop in L_2 norm of the error residual for each of the subdivided zones. Although a 6 deg angle of attack is small relative to what the aircraft can achieve in flight, it is large enough to generate the fluid phenomena of interest. Grid clustering in the directions normal to the aircraft surface provided adequate definition of the boundary layer, with the first point off the surface in or near the viscous sublayer, typically at a y^+ value of 5–8.

As shown in Fig. 3, the computer results are quantitatively in good agreement with the experimental pressure coefficient distributions on the fuselage centerline and at four spanwise stations on the wing. The compression and expansion over the canopy, the suction peak near the leading edge, and the oblique/normal shock combination near the wingtip are all

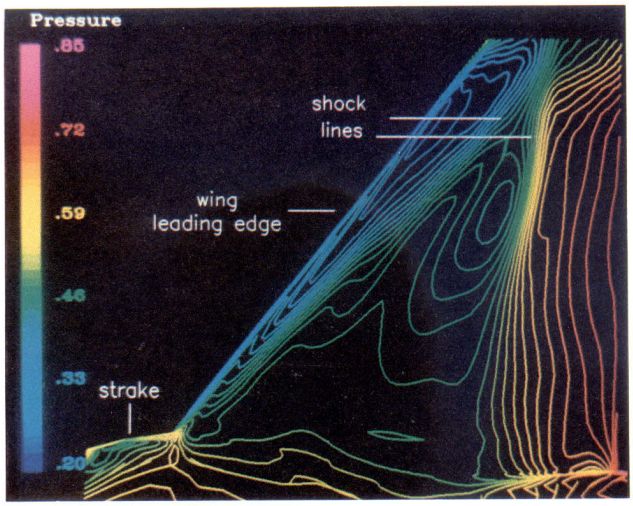

Fig. 4 Computed pressure contours on the wing-fuselage planform for turbulent cases; $M_\infty = 0.9$, $\alpha = 6.15$ deg, $Re = 4.5 \times 10^6$.

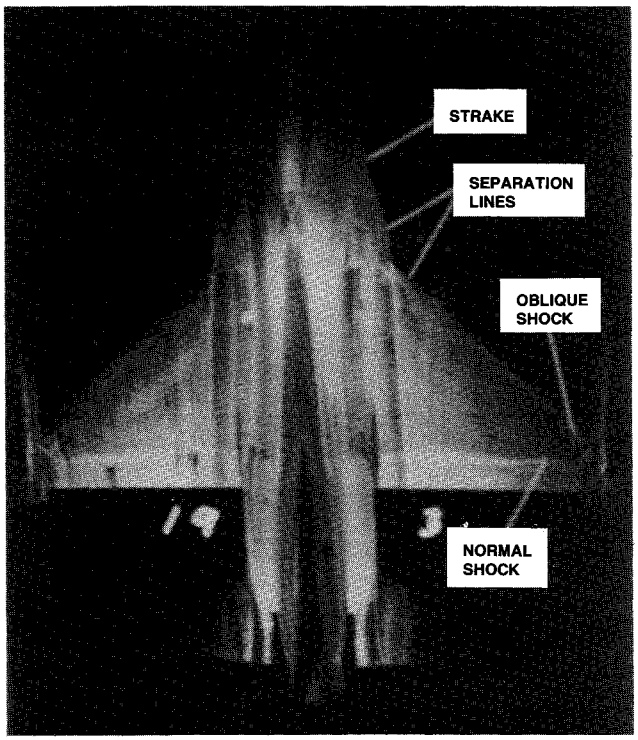

Fig. 5 F-16A wind-tunnel oil-flow visualization; $M_\infty = 0.9$, $\alpha = 6.15$ deg, $Re = 4.5 \times 10^6$.[20]

captured. Finer streamwise resolution, to be used in forthcoming grids, is needed to improve the accuracy of their depiction. Preliminary computations[22] indicate that, with increased resolution, the computed aft normal shock will extend farther inboard, in better agreement with experiment. The shock features of this solution are well detailed by the computed surface pressure contours near the boundary-layer edge shown in Fig. 4. Experimental oil-flow visualization for these conditions[20] is shown in Fig. 5. Crossflow velocity vectors are shown in Fig. 6. Examination of the core region reveals the clockwise flow direction of the vortex.

Laminar Cases, $\alpha = 10$ deg

A quasilaminar subsonic solution was obtained for $M_\infty = 0.6$, $\alpha = 10$ deg, and $Re = 8.0 \times 10^6$. Although the Reynolds number is well above the expected transition value, the turbulence model was not employed because it would not

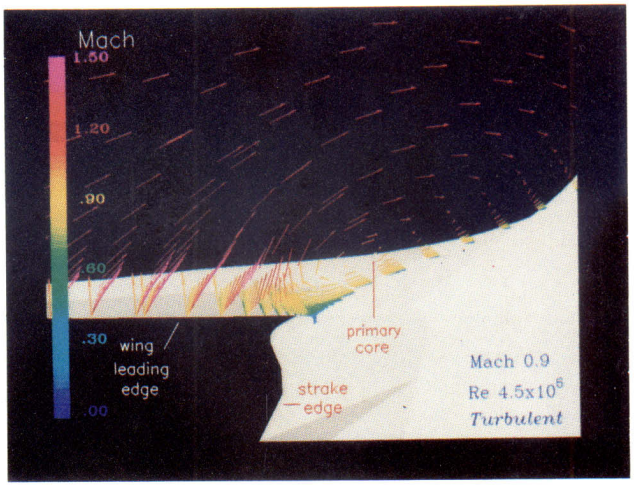

Fig. 6 Computed crossflow velocity vectors above the strake; $M_\infty = 0.9$, $\alpha = 6.15$ deg, $Re = 4.5 \times 10^6$ (turbulent case).

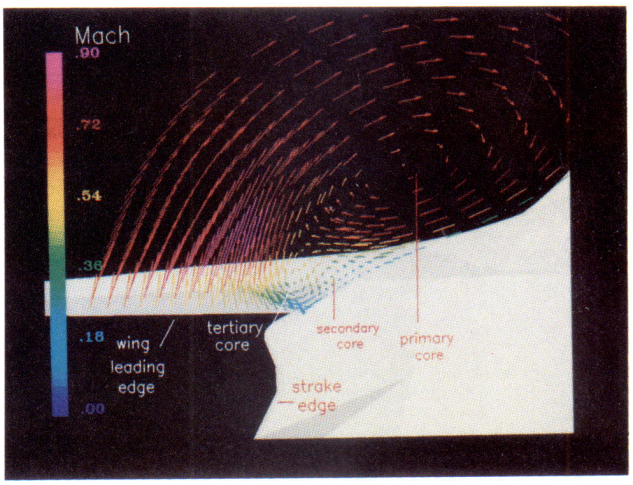

Fig. 7 Computed crossflow velocity vectors above the strake; $M_\infty = 0.6$, $\alpha = 10.0$ deg, $Re = 8.0 \times 10^6$ (quasilaminar case).

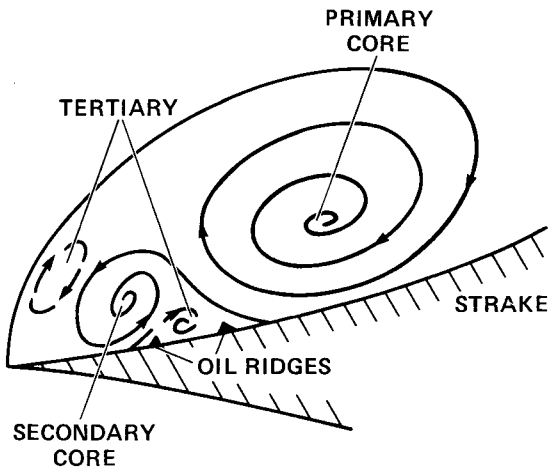

Fig. 8 Crossflow topology of vortical interactions above strake.

have been effective with the slightly coarsened grid required to converge the solution in this higher incidence case. It took 1200 iterations to drop the error residual over three orders of magnitude in all zones, at a cost of 6 CPU h of Cray XMP/48 times. Laminar cases were computed using $R_e = 1.5 \times 10^4$ to match water-tunnel test conditions for comparison with flow visualization.[23]

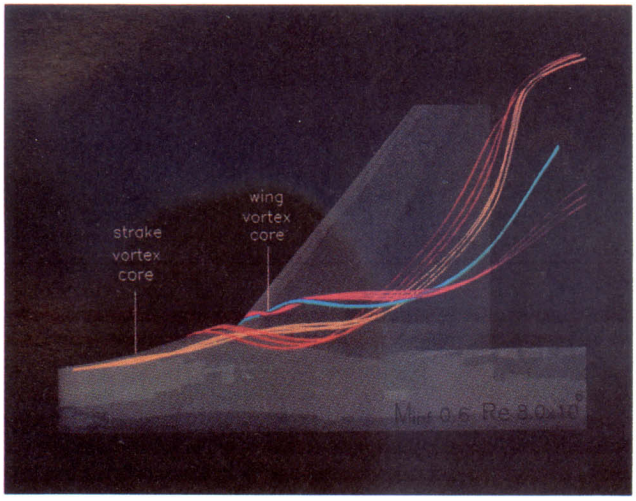

Fig. 9 Unrestricted vortex-interaction particle traces for $M_\infty = 0.6$, $\alpha = 10.0$ deg, $Re = 8.0 \times 10^6$ (quasilaminar case).

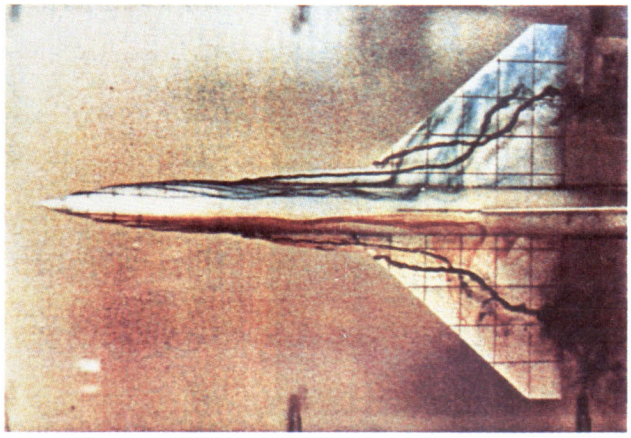

Fig. 10 F-16A-like water-tunnel flow visualization; $\alpha = 15.0$ deg, $Re = 1.5 \times 10^4$.[27]

Crossflow velocity vectors for this case are shown in Fig. 7. The viewpoint is the same as that used in Fig. 6. The strake-generated vortex appears to be located farther from the strake-wing juncture surface than was the case for $M_\infty = 0.9$, $\alpha = 6$ deg (Fig. 6). This vortex also has a more visible interaction with the high-velocity flow over the wing leading edge, and with the boundary layer. Close examination of the velocity vectors underneath the clockwise-rotating primary vortex reveals a counterclockwise-rotating secondary vortex, and adjacent to it a clockwise-rotating tertiary construction. A diagram depicting the relationship between these vortical structures is shown in Fig. 8, which was adapted from a drawing by Luckring[24] for an experimental strake-wing investigation. The magenta-colored velocity vectors in Fig. 7 suggest the interaction of the high-velocity flow over the leading edge, which is further accelerated by the vortical strake-flow.

Water-Tunnel Flow-Visualization Comparisons

Both Wortman[25] and Erickson[26] have warned against relying on water-tunnel flow visualization for comparison to high-Reynolds-number experiments and solutions. Erickson in particular cautioned that low-angle-of-attack comparisons were invalid because the entrainment of turbulent fluid from the wake causes premature vortex bursting. He suggests that for higher angles of attack, for example, above $\alpha = 10$ deg, and for higher leading-edge sweep angles, the comparisons have more validity. In this regime, the flows are vortex-dominated, and boundary-layer effects, which are Reynolds-number-sensitive, are not so significant. For these reasons, the following comparisons have been used as a guide to understanding the interaction process, rather than as a definitive indicator of the flow behavior at higher Reynolds numbers.

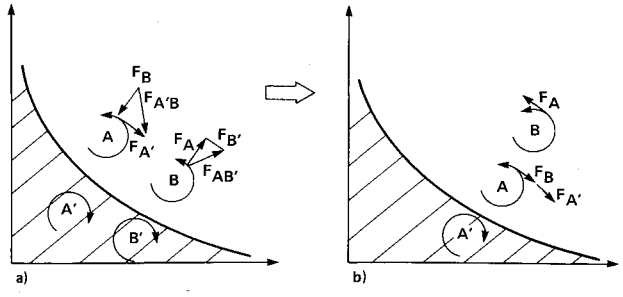

Fig. 11 Vortex-interaction schematic in crossflow plane at a) strake-wing juncture, and b) downstream, as viewed from behind.

Computed particle traces for this quasilaminar case are shown in Fig. 9. The particles are released at selected points near the body surface and are allowed to move freely in all directions. Figure 9 shows that the strake vortex, indicated by yellow traces at the core surrounded by red traces on the periphery, is pulled spanwise underneath the wing-root or wing leading-edge vortex, which is represented by a blue core circulated by magenta traces. This representation compares favorably with the water-tunnel flow visualization shown in Fig. 10, which was obtained by Malcolm and Skow[27] for an F-16-like geometry with an extended fuselage and a more highly swept wing.

A schematic examination of vortical interaction in the crossflow plane, as drawn in Fig. 11 for two stages in the evolution, suggests why the strake vortex A is forced under the wing-root vortex B, and both move outboard spanwise. This perspective is from downstream and above the trailing edge, and represents what might develop from the initial interactions of the vortices near the leading edge, to where they might wind around each other near the trailing edge; strake vortex A feels the downward force of wing-root vortex B, combined with the spanwise and downward force of fuselage mirror-vortex A'. Vortex B feels the upward force of vortex A, along with the spanwise force of mirror-vortex B'. Other mirror effects are deemed to be secondary because of distance from A or B. It is also probable that the strake vortex is weakening because of the distance traveled from its formation and resultant dissipation, whereas the wing-root vortex is both nearer to its source and is fed by a stronger source.

In order to gain further insight into the behavior and interaction of the strake and wing vortices, a water-tunnel test was carried out in cooperation with Malcolm and Schiff[21] in the Ames-Dryden Flow Visualization Facility (FVF). The model used was an F-16A, with the exception that the empennage area was removed. The water-tunnel model had a flowthrough inlet capability, and tests were conducted over a range of inlet-flow conditions. The experimental dye traces more closely matched the computed particle traces when the inlet flow was completely blocked, better simulating the pressure buildup caused by the faired-over inlet. The comparison to computation is still not that good, suggesting that the inlet and aft fuselage differences are significant.

A laminar solution was computed at the Reynolds number, $Re = 1.5 \times 10^4$, but with $M_\infty = 0.6$. Particles were released from the same locations as those in Fig. 9. The Mach number increase appeared to shift the particle traces farther inboard spanwise but did not modify the basic interaction between the strake-generated and wing-root vortices.

Other water-flow visualization studies display a significant vortex interaction for similar configurations. One is a water-sled hydrogen-bubble flow visualization obtained by Thompson,[28] for a double-delta wing at slightly higher angle of attack. Flow visualization for an F-16A geometry at $\alpha = 8$ deg, obtained by Erickson,[26] suggests entrainment of the strake vortex by the wing-root vortex.

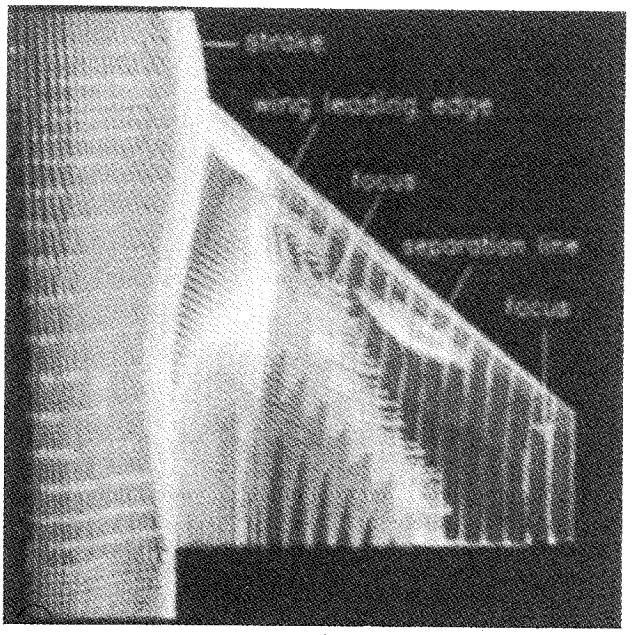

Fig. 12 Computed surface-particle traces; $M_\infty = 0.6$, $\alpha = 10.0$ deg, $Re = 8.0 \times 10^6$ (quasilaminar).

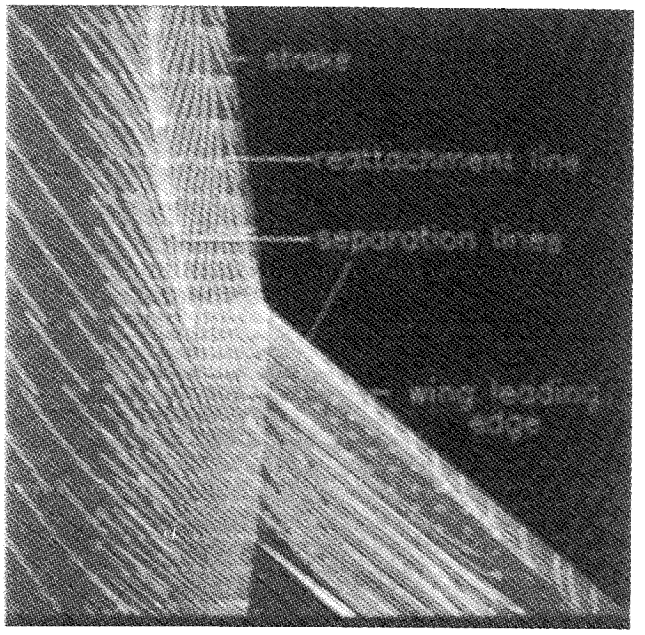

Fig. 13 Detail of computed surface-particle traces in strake-wing juncture region; $M_\infty = 0.6$, $\alpha = 10.0$ deg, $Re = 8.0 + 10^6$ (quasilaminar).

Although the water-tunnel flow visualization described in the above experiments does not rigorously match the behavior of the computer particle traces, the same fundamental vortical convection and interaction processes are captured by both, with variations because of Reynolds number, Mach number, and configuration differences. The differences in the vortex interactions of the flowthrough vs the blocked-inlet experiment highlight the importance of including the flowthrough inlet, with proper mass flow conditions, in the computations.

Critical-Point Analysis

The nature of these separated flowfields begs topological analysis, grounded on the framework initiated by Legendre[29] for streamlines immediately adjacent to the surface. Legendre's approach treats the flowfield as a continuous vector field. Under this approach, a given flowfield can be categorized mathematically in terms of its critical points, such as nodes, foci, and saddle points. This method of analysis was tailored to viscous flows by Lighthill,[30] who treated a continuous vector field of skin friction lines rather than limiting streamlines. The utility of this approach becomes manifest when one views surface oil-flow visualization, which can be treated as skin-friction lines. Tobak and Peake,[31,32] Peake and Tobak,[33,34] Dallmann,[35] Perry and Fairlie,[36] and others have developed a wide variety of insights and offered a topological grammar of interaction rules for the relationships occurring within these topological maps. Certain combinations of nodes, saddle points, and lines of attachment and separation are required by the assumption that the flow is a continuous vector field. The surface oil-flow pattern can then be examined to determine the formation of vortical constructions. Their interaction with other flow features can be limited and categorized based on this flow grammar.

Surface-particle traces are the computational analogy of experimental oil-flow visualizations, since the particles are released just above the body surface and move with the local flow velocity. Surface-particle traces for the solution computed at $M_\infty = 0.6$, $\alpha = 10$ deg, and $Re = 8.0 \times 10^6$ are displayed in Fig. 12. The relationship of the two counter-rotating foci evident in Fig. 12 is typical for a low-aspect-ratio wing at moderate angles of attack. When the two are separated by a node, which is not the case here, a "mushroom cap"-type of separated region is typically detected. Figure 13 depicts an enlarged detail of the strake-wing juncture area of the computed particle traces shown in Fig. 12. It is noteworthy that

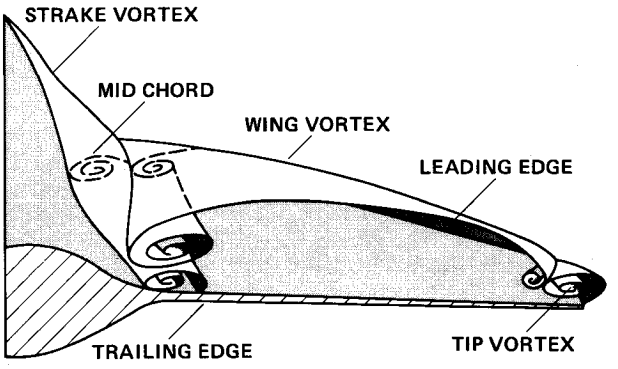

Fig. 14 Vortical schematic of primary flow properties above the wing; $M_\infty = 0.6$, $\alpha = 10.0$ deg, $Re = 8.0 \times 10^6$ (quasilaminar).

the separation line near and parallel to the wing leading edge detected in the oil-flow visualization of Fig. 5, is captured in these computed particle traces. Topological analyses of Figs. 12 and 13 emphasizing the appropriate secondary vortex separation and reattachment line relationships have been accomplished (see Ref. 37). The schematic in Fig. 14 displays the fundamental fluid interactions occurring above the wing-fuselage for this solution.

A videotape of the dye movement, made during the water-tunnel test, has proven invaluable in developing perspective for what has been computed. If a flowfield interpretation like this properly balances the relative positions and numbers of nodal and saddle points, and violates none of the generally accepted rules of topological grammar, it strengthens support for the likelihood that the computed solution captures the flow physics correctly. If, in addition, the surface-particle traces properly match surface oil-flow visualization topography for identical flow parameters, then the correctness of the computed result is confirmed.

Conclusions

The thin-layer Navier-Stokes equations were solved for flowfield around a wing-strake-fuselage configuration similar to the General Dynamics F-16A aircraft. Steady-state solutions were obtained at angles-of-attack ranging from 6 to 10 deg at $M_\infty = 0.3$, 0.6, and 0.9, and Reynolds numbers matching those of wind-tunnel and water-tunnel experiments.

The flowfield was divided into multiple blocks using a zoning program; the TNSWF solution program, based on an implicit solution algorithm, updates each subregion of the flowfield sequentially. The total grid contained approximately 300,000 grid points, and clustering was effected normal to all aircraft surfaces.

The computed solutions agree well quantitatively with wind-tunnel pressure-distribution data, and they agree well qualitatively with dye-flow visualization from water-tunnel tests. Of primary interest is the correct capture of the strake-generated vortex, and its interaction with the wing-generated vortex at $\alpha = 10$ deg. This approach holds great promise for future evaluation of more detailed geometries. An effort to compute a similar configuration with the flowthrough inlet modeled is nearing completion.

A more complete description of the work described in this paper may be gained from perusal of Ref. 37.

Acknowledgments

The authors would like to thank Dr. Thomas Edwards and Reese Sorenson of NASA Ames Research Center for their help in providing the surface fitting and coarse grid for the F-16 aircraft; Mr. Scott Rudin of General Dynamics for his generosity in retrieving archived data and flow-visualization materials; Mr. Jerry Malcolm of Eidetics International and Dr. Lewis Schiff of NASA Ames Research Center for their assistance in running the water-tunnel test; and Ms. Karen L. Gundy of NASA Ames, Mr. Jason Williams and Mrs. Alice Barlow of Sterling Software for their assistance with graphical technique development and application.

References

[1]Peake, D. J. and Tobak, M., "On Issues Concerning Flow Separation and Vortical Flows in Three Dimensions," NASA TM-84374, May 1983.

[2]Chapman, D. R., "Computational Aerodynamics: Review and Outlook," *AIAA Journal*, Vol. 17, Dec. 1979, pp. 1293–1313.

[3]Rubbert, P. E. and Sarris, G. R., "Review and Evaluation of a Three-Dimensional Lifting Potential Flow Analysis Method for Arbitrary Configurations," AIAA Paper 72-188, Jan. 1972.

[4]Holst, T. L. and Thomas, S. D., "Numerical Solution of Transonic Wing Flowfields," *AIAA Journal*, Vol. 21, June 1983, pp. 863–870.

[5]Newsome, R. W., "A Comparison of Euler and Navier-Stokes Solutions for Supersonic Flow over a Conical Delta Wing," AIAA Paper 85-0111, Jan. 1985.

[6]Murman, E. M. and Rizzi, A., "Applications of Euler Equations to Sharp Edge Delta Wings with Leading Edge Vortices," *AGARD Symposium on Application of Computational Fluid Dynamics in Aeronautics*, Aux-En-Provence, France, April 1986, p. 15.11.

[7]Westphal, R. V., Eaton, J. K., and Pauley, W. R., "Interaction Between a Vortex and a Turbulent Boundary Layer in a Streamwise Pressure Gradient," *5th Symposium on Turbulent Shear Flows*, Cornell Univ., Ithaca, NY, Aug. 1985, pp. 7.1–7.5.

[8]Baldwin, B. S. and Lomax, H., "Thin Layer Approximation and Algebraic Model for Separated Turbulent Flows," AIAA Paper 78-257, Jan. 1978.

[9]Steger, J. L., "Implicit Finite Difference Simulation of Flow About Arbitrary Geometries with Application to Airfoils," AIAA Paper 77-665, June 1977.

[10]Pulliam, T. H., "Euler and Thin-Layer Navier-Stokes Codes: ARC2D, and ARC3D," Notes for the Computational Fluid Dynamics Users' Workshop, Univ. of Tennessee Space Institute, Tullahoma, TN, March 1984.

[11]Beam, R. M. and Warming, R. F., "Implicit Numerical Methods for the Compressible Navier-Stokes and Euler Equations," Lecture Notes, The 1981–82 Lecture Series Programme, Computational Fluid Dynamics, von Kármán Institute for Fluid Dynamics, Rhode-Saint-Genese, Belgium, March–April 1982.

[12]Pulliam, T. H. and Chaussee, D. S., "A Diagonal Form of an Implicit Approximate-Factorization Algorithm," *Journal of Computational Physics*, Vol. 39, Feb. 1981, pp. 347–363.

[13]Flores, J., "Convergence Acceleration for a Three-Dimensional Euler/Navier-Stokes Zonal Approach," AIAA Paper 85-1495, July 1985.

[14]Hung, C. M. and MacCormack, R. W., "Numerical Simulation of Supersonic and Hypersonic Turbulent Compression Corner Flows," *AIAA Journal*, Vol. 15, March 1977, pp. 410–416.

[15]Holst, T. L., Kaynak, U., Gundy, K. L., Thomas, S. D., and Flores, J., "Numerical Solution of Transonic Wing Flows Using an Euler/Navier-Stokes Zonal Approach," AIAA Paper 85-1640, July 1985.

[16]Flores, J., Holst, T. L., Kaynak, U., Gundy, K., and Thomas, S. D., "Transonic Navier-Stokes Wing Solution Using a Zonal Approach: Part 1. Solution Methodology and Code Validation," AGARD Paper 30A, *AGARD Symposium on Applications of Computational Fluid Dynamics in Aeronautics*, Aux-En-Provence, France, April 1986.

[17]Kaynak, U., Cantwell, B. J., and Holst, T. L., "Numerical Simulation of Transonic Separated Flows Over Low-Aspect Ratio Wings," AIAA Paper 86-0508, Jan. 1986.

[18]Edwards, T. A., "Geometry Definition and Grid Generation for a Complete Fighter Aircraft," Paper 4, *AGARD Symposium on Application of Computational Fluid Dynamics in Aeronautics*, Aux-En-Provence, France, April 1986.

[19]Sorenson, R. L., "Three-Dimensional Elliptic Grid Generational About Fighter Aircraft for Zonal Finite-Difference Computations," AIAA Paper 86-0429, Jan. 1986.

[20]Hammond, D. G., "Wind Tunnel Data Report 16PR135, 1/9-Scale F-16 Pressure Loads Test, AEDC, 16-T Test TF-397 (Phase I and II), Runs 35–81," Arnold Engineering Dev. Center, Tullahoma, TN, Jan. 1976.

[21]Malcolm, G. N., Schiff, L. B., and Reznick, S. G., Unpublished results of water-tunnel tests, NASA Ames-Dryden, July 1986.

[22]Flores, J., Reznick, S. G., Holst, T. L., and Gundy, K. L., "Transonic Navier-Stokes Solutions for a Fighter-like Configuration," AIAA Paper 87-0032, Jan. 1987.

[23]Srinivasan, G. R., McCroskey, W. J., Baeder, J. D., and Edwards, T. A., "Numerical Simulation of Tip Vortices of Wings in Subsonic and Transonic Flows," AIAA Paper 86-1095, May 1986.

[24]Luckring, J. M., "Flow Visualization Studies of a General Research Fighter Model Employing a Strake-Wing Concept at Subsonic Speeds," NASA TM-80057, Aug. 1979.

[25]Wortman, A., "On Reynolds Number Effects in Vortex Flow Over Aircraft Wings," AIAA Paper 84-0137, Jan. 1984.

[26]Erickson, G. E., "Vortex Flow Correlation," Air Force Wright Aeronautical Labs., TR-80-3413, U.S. Air Force, Jan. 1981, pp. 176–180.

[27]Malcolm, G. N. and Skow, A. M., "Improved High Angle of Attack Controllability Through Vortex Manipulation," Eidetics International, Inc., Topic 30, contracted for Air Force Wright Aeronautical Labs., TR-86-101, Jan. 1986.

[28]Thompson, D. H., "A Visualization Study of the Vortex Flow Around Double-Delta Wings," ARL-AERO-R-165, Department of Defense, Commonwealth of Australia, Aug. 1985.

[29]Legendre, R., "Separation de l'ecoulement laminaire tridimensionnel," *Rech, Aero.*, Vol. 54, 1956, pp. 3–8.

[30]Lighthill, M. J., "Attachment and Separation in Three-Dimensional Flow," *Laminary Boundary Layers*, ed. L. Rosenhead, II, 2.6: Oxford Univ. Press, 1963, pp. 72–82.

[31]Tobak, M. and Peake, D. J., "Topology of Two-Dimensional and Three-Dimensional Separated Flows," AIAA Paper 79-1480, July 1979.

[32]Tobak, M. and Peake, D. J., "Topology of Three-Dimensional Separated Flows," NASA TM-81294, April 1981.

[33]Peake, D. J. and Tobak, M., "Three-Dimensional Interactions and Vortical Flows With Emphasis on High Speeds," NASA TM-81169, March 1980.

[34]Peake, D. J. and Tobak, M., "Three-Dimensional Flows About Simple Components at Angle of Attack," NASA TM-84226, March 1982.

[35]Dallmann, U., "Topological Structures of Three-Dimensional Vortex Flow Separation," AIAA Paper 83-1735, July 1983.

[36]Perry, A. E. and Fairlie, B. D., "Critical Points in Flow Patterns," *Advances in Geophysics*, Vol. 18B, Academic Press, 1974, pp. 299–315.

[37]Reznick, S. G., "Transonic Navier-Stokes Computations of Strake-Generated Vortex Interactions for a Fighter-Like Configuration," NASA TM-100009, Feb. 1988.